Published in final edited form as:
J Biol Chem. 2003 April 11; 278(15): 13496–13502. doi:10.1074/jbc.M213150200.

A Catalytic Mechanism for D-Tyr-tRNA^{Tyr} Deacylase Based on the Crystal Structure of *Hemophilus influenzae* HI0670*

Kap Lim[‡], **Aleksandra Tempczyk**[‡], **Nicklas Bonander**[§], **John Toedt**[‡,¶], **Andrew Howard**[‖,**], **Edward Eisenstein**[‡,‡‡], and **Osnat Herzberg**[‡,§§]

[‡]Center for Advanced Research In Biotechnology, University of Maryland Biotechnology Institute, Rockville, Maryland 20850

[§]The National Institute of Standards and Technology, Gaithersburg, Maryland 20899

[‖]Advanced Photon Source, Argonne National Laboratory, Argonne, Illinois 60439

[**]Department of Biological, Chemical, and Physical Science, Illinois Institute of Technology, Chicago, Illinois 60616

[‡‡]Department of Chemistry and Biochemistry, University of Maryland Baltimore County, Baltimore, Maryland 21250

Abstract

D-Tyr-tRNA^{Tyr} deacylase is an editing enzyme that removes D-tyrosine and other D-amino acids from charged tRNAs, thereby preventing incorrect incorporation of D-amino acids into proteins. A model for the catalytic mechanism of this enzyme is proposed based on the crystal structure of the enzyme from *Haemophilus influenzae* determined at a 1.64-Å resolution. Structural comparison of this dimeric enzyme with the very similar structure of the enzyme from *Escherichia coli* together with sequence analyses indicate that the active site is located in the dimer interface within a depression that includes an invariant threonine residue, Thr-80. The active site contains an oxyanion hole formed by the main chain nitrogen atoms of Thr-80 and Phe-79 and the side chain amide group of the invariant Gln-78. The Michaelis complex between the enzyme and D-Tyr-tRNA was modeled assuming a nucleophilic attack on the carbonyl carbon of D-Tyr by the Thr-80 O^{γ} atom and a role for the oxyanion hole in stabilizing the negatively charged tetrahedral transition states. The model is consistent with all of the available data on substrate specificity. Based on this model, we propose a substrate-assisted acylation/deacylation-catalytic mechanism in which the amino group of the D-Tyr is deprotonated and serves as the general base.

Aminoacyl-tRNA synthetases transfer L-amino acids to tRNA, and the aminoacyl-tRNAs are delivered to the ribosome where protein synthesis takes place. These enzymes may also utilize D-amino acids that if incorporated into a polypeptide chain would impair correct folding. To maintain high fidelity of protein synthesis, any incorrectly charged tRNA must be removed. D-Tyr-tRNA^{Tyr} deacylase hydrolyzes the ester link between D-Tyr and tRNA (1, 2). Found in many bacteria as well as in Saccharomyces cerevisiae, Caenorhabditis elegans, Arabidopsis thaliana, mouse, and human, the enzyme also acts on D-Asp, D-Trp, D-Ser, D-Leu, D-Gln, D-Phe, and D-Gly tRNAs (1-4). Whereas the enzyme exhibits broad specificity toward D-amino acids, it is inactive toward L-aminoacylated tRNAs (1) and *N*-blocked D-aminoacylated tRNAs (2).

---

*This work was supported by National Institutes of Health Grant PO1 GM57890.

[§§]To whom correspondence should be addressed. Tel.: 301-738-6245; Fax: 301-738-6255; osnat@carb.nist.gov..
[¶]Present address: Dept. of Physical Science, Eastern Connecticut State University, Willimantic, CT 06226.

Recently, the crystal structure of D-Tyr-tRNA^{Tyr} deacylase from *Escherichia coli* has been determined (5), revealing a dimeric structure and a novel fold. Ferri-Fioni *et al.* (5) propose that the active site is formed in a depression at the dimer interface that contains a cluster of invariant residues including residues 77–81 (SQFTL) of one monomer and Arg-7 and residues 134–140 (N*X*G(V/F)T) of the second monomer. They also proposed that conserved positively charged residues at positions 48, 53, 87, and 90 interact with negatively charged phosphate groups on the tRNA. However, none of the publications so far present a proposal for the catalytic mechanism.

The D-Tyr-tRNA^{Tyr} deacylase structure from *Haemophilus influenzae* (HI0670 according to the The Institute for Genomic Research (TIGR) numbering scheme (6)) reported here is similar to that from *E. coli*. A comparison of the two structures together with modeling of the enzyme/D-Tyr-tRNA complex provides the structural basis for a proposed catalytic mechanism and explains all of the enzyme specificity data that have been reported.

MATERIALS AND METHODS

Protein Production

The gene encoding HI0670 was amplified from chromosomal DNA of *H. influenzae* Rd KW20 and cloned into the pET17b (Novagen) for expression of the native polypeptide in *E. coli* strain BL21(DE3). Cells were grown at 37 °C in LB medium containing 100 μg/ml ampicillin. At mid-log phase (A_{600} = 0.8), expression was induced by the addition of 1 mM isopropyl-1-thio-β-D-galactopyranoside and growth continued for 4 h. Harvested cells were suspended in 20 mM Tris-HCl, pH 8.4, and lysed with three passes at 8,000–10,000 p.s.i. in a French press.

After clarification of the cell lysate by high speed centrifugation, the protein was purified with the use of a BioCAD 700E chromatography work station (PerSeptive Biosystems). The purification protocol consisted of two steps. The first step employed an anion exchange column (Poros HQ 50) at pH 8.4, and the second step employed a cation exchange column (Poros HS 20) at pH 8.0. The integrity of the purified protein was assessed by polyacrylamide gel electrophoresis in the presence of SDS. The pooled fractions of HI0670 were concentrated (~3 mg/ml) and dialyzed at 4 °C against solution containing 50 mM Tris-HCl, pH 7.5, 0.1 mM dithiothreitol, and 0.1 mM EDTA. Protein crystals suitable for x-ray diffraction work were formed during dialysis. The molecular weight of HI0670 was verified by MALDI mass spectrometry (Voyager, PerSeptive Biosystems) (M_r = 15,861.7 observed and 15,862.3 calculated). Thermal stability was examined with the use of circular dichroism at 208 nm, revealing a stable protein with a T_m = 64 °C. The protein exists in solution predominantly in dimeric form as determined by sedimentation equilibrium measurement.

It is worth noting that our initial attempts to express the HI0670 as a thrombin-cleavable His-tagged protein resulted in an insoluble product. With hindsight, the folding of the polypeptide chain was impaired because the N-terminal amino group is buried and forms essential contacts with three carboxylate groups.

Structure Determination

The HI0670 crystals belong to space group $P4_12_12$, and the asymmetric unit contains 1 molecule and 55% solvent. For diffraction data collection, crystals were flash-cooled at 100 K from a solution containing the dialysis buffer and 20% glycerol. Data were collected using both a home x-ray facility and the IMCA-CAT 17-ID beamline at the Advanced Photon Source (Argonne National Laboratory, Argonne, IL). The home CuK_α x-ray source was a Siemens rotating anode equipped with MAR345 image plate. The IMCA-CAT beamline

was equipped with a MAR CCD detector. Data processing was performed using the HKL program suite (7).

A single crystal was soaked with buffer containing 4 mM ethyl mercury phosphate for 2 days, and 2.0-Å resolution diffraction data were collected on the home x-ray source. The data were non-isomorphous with the native data; thus, the phases were determined using solely the mercury anomalous signal. The statistics of data collection are shown in Table I.

Computations leading to phase determination were carried out with the CCP4 suite of computer programs (8). The mercury-derivative anomalous difference Patterson map revealed a single peak (>8 σ). The computer program MLPHARE (9) was used to refine the position and occupancy of the heavy atom and to calculate phases. The phases were further improved by solvent-flattening using the computer program DM (10). The resulting electron density map was excellent, showing the molecular boundaries, unambiguous secondary structural elements, and clear density for the side chains. Most of the 144-residue polypeptide chain (93%) was traced automatically using the computer program Arp/Warp (11). Building of the remaining residues and adjustments to the model were carried out with the interactive computer graphics program O (12) on a Silicon Graphics Octane work station.

Following the structure determination, a native data set was collected to a resolution of 1.64Å on the IMCA-CAT beamline (Table I) and used for structure refinement. Refinement of the HI0670 structure was carried out using the CNS program (13) with the data between 20.0 and 1.64 Å for which $F \geq 2\sigma(F)$ (Table II). In the final stages of the refinement, water molecules were added to the model based on the $F_o - F_c$ difference electron density map (where F_o and F_c are the observed and calculated structure factors, respectively) using peaks with a density of ≥3σ as the acceptance criteria.

Modeling

A model of the enzyme/D-Tyr-tRNA^{Tyr} complex was built on a Silicon Graphics Octane work station using the computer program TURBO-FRODO (14). Because no structure for tRNA^{Tyr} is available, the structure of yeast tRNA^{Phe} (Protein Data Bank code 1ehz) (15) was used. *H. influenzae* tRNA^{Tyr} contains 85 nucleotides, whereas tRNA^{Phe} of both yeast and *H. influenzae* contain 76 nucleotides (www.tigr.org). Thus, structural differences between the two are expected. Yet, all of the known tRNA structures have a similar L-shaped structure with an unpaired 3′-terminal CCA sequence at the acceptor stem. It is the 3′-CCA region that is expected to undergo conformational changes to fit in the active site of the deacylase. The D-Tyr-tRNA was built by linking D-tyrosine to the O3′ atom of adenosine 76 (A76). After manual adjustments to the 3′-CCA-D-Tyr conformation as described under "Results and Discussion," energy minimization of the modeled tRNA was carried out using CNS.

RESULTS AND DISCUSSION

HI0670 Structure

The final model of HI0670 includes all 144 amino acid residues and 207 water molecules. The quality of the electron density map is shown in Fig. 1, focused on the region of the proposed active site. For the mercury-soaked crystal, the data show that the mercury atom is bound to Cys-133. The N-terminal amino group (Met-1) is buried, interacting with the carboxyl groups of Glu-34, Asp-37, and the C terminus.

The molecules pack into closely associated dimers around the 2-fold crystallographic symmetry axis (Fig. 2). The fold is the same as that of the *E. coli* D-Tyr-tRNA deacylase

(Protein Data Bank code 1jke) (5). Each monomer contains a five-stranded mixed twisted β-sheet and a three-stranded anti-parallel β-sheet. The dimer packing results in the three-stranded β-sheets of two monomers forming a continuous six-stranded anti-parallel β-sheet, and the pair of five-stranded β-sheets forms a β-sandwich with a central axis roughly perpendicular to the six-stranded β-sheet. Two parallel α-helices cover each of the five-stranded β-sheets. A large loop (residues 83-94) extends from each monomer to interact with the neighboring molecule. Although Ferri-Fioni *et al.* (5) list structural similarities between portions of the molecule and segments of other proteins (5), we note that these correspond to small common motifs and are not extensive enough to imply evolutionary relationship. Thus, based on Dali (16), the fold is unique to D-Tyr-tRNA deacylase.

The *H. influenzae* and *E. coli* deacylases share a 67% sequence identity, and their polypeptide chains align well with one another. Excluding one residue that is deleted in *H. influenzae* HI0670 compared with the *E. coli* enzyme (residue 117), the superposition of the Cα atoms of the monomers results in root mean square (r.m.s.)[1] deviation of 0.6 Å, and for the respective dimers (using dimer AD of the *E. coli* enzyme structure), the r.m.s. deviation is 0.5 Å. When dimer BC of the *E. coli* deacylase structure is compared, the r.m.s. deviation values for monomers and dimers are 0.7 and 0.6 Å, respectively.

The positions of some water molecules are also conserved in the *H. influenzae* and *E. coli* enzyme structures. The superposition of HI0670 and the *E. coli* AD dimers shows seven pairs of water molecules within 0.2 Å, 15 pairs within 0.2–0.5 Å, and 25 pairs within 0.5–1.0 Å. For the BC dimer, there are 4, 18, and 23 paired water molecules within the corresponding distances. The best matched water molecules are either buried or involved in bridging hydrogen bonds between protein main chain atoms.

Active Site

As reported earlier (5), multiple sequence alignment (Fig. 3) and structure analysis show a cluster of invariant residues located in a surface depression at a dimer interface region. The dimer contains two such sites ~20 Å apart on the opposite sides of the dimer interface, and these are probably the active sites of the enzyme. In the following discussion, residues located on the symmetry-related molecule are labeled by an *asterisk*.

Much of the postulated active site depression is lined with hydrophobic residues including four phenylalanines, Phe-79, Phe-93, Phe-124, and Phe-140* (Fig. 4*A*). Invariant polar residues in the active site are Arg-7*, Ser-77, Gln-78, and The-80. Ferri-Fioni *et al.* (5) also noted four conserved positively charged residues, two at the edge of the putative active site (Arg/Lys-53* and Lys-90) and two at a more remote location (Arg/Lys-48* and Lys-87, although position 87 is some-times occupied by a serine or an alanine), which may play a role in tRNA recognition. Although they identify the location of the active site, the authors did not suggest which are the catalytic residues nor did they propose a catalytic mechanism. Structural considerations, modeling, and inferences from the mechanisms of other hydrolytic enzymes enabled us to develop a proposal for the catalytic mechanism as described below.

Proposed Michaelis Complex and Catalytic Mechanism

Enzyme-catalyzed hydrolysis often involves a general base mechanism with an enzyme group mounting a nucleophilic attack on a carbonyl carbon atom of the substrate and a group that serves as a proton park, enabling shuttling of protons from and to the nucleophilic group during catalysis. This is a two-step reaction with an acyl enzyme intermediate and two tetrahedral transition states, one en route to the acyl enzyme intermediate and the second

[1]The abbreviation used is: r.m.s., root mean square.

along the deacylation step when the hydrolytic water molecule attacks. We propose that D-Tyr-tRNA^{Tyr} deacylase utilizes such a general base mechanism. Two invariant residues in the active site need to be considered as potential nucleophilic groups, Ser-77 and Thr-80. Ser-77 is rather buried, whereas Thr-80 is accessible to solvent. Moreover, a striking oxyanion hole is located adjacent to Thr-80 (but not adjacent to Ser-77) formed by the side chain amide group of the invariant Gln-78 and the main chain nitrogen atoms of Phe79 and Thr80 (Fig. 4*A*). The presence of an oxyanion hole is reminiscent of the catalytic machinery of other hydrolytic enzymes such as the serine and thiol proteases and the serine β-lactamases (17, 18). Similarly to Gln-78 of the deacylase, a glutamine or an asparagine amide group participates in the formation of the oxyanion hole in papain and subtilisin, respectively. The oxyanion hole plays a role along the reaction pathway by stabilizing the negatively charged transition states.

With these considerations in mind, the Michaelis complex between HI0670 and the aminoacyl-tRNA was modeled following the hypothesis that Thr-80 is the nucleophilic group. Note that in the *E. coli* enzyme structure, the oxyanion hole of molecule A is shielded from solvent by Phe-79 side chain adopting a conformation different from that seen in molecule D or in the structure of HI0670. We propose that the active conformation is the one exposing the oxyanion hole to solvent.

To enable nucleophilic attack, the χ_1 dihedral angle of Thr-80 was rotated by 120° so that the O$^{\gamma}$ atom is accessible to solvent. The tRNA molecule (consisting of the 76-nucleotide-long tRNA^{Phe}) linked to D-Tyr via an ester bond on the O3′ of ribose 76 was manually positioned so that the carbonyl group of the D-Tyr faced the Thr-80 O$^{\gamma}$ atom and the oxygen atom was accommodated in the oxyanion hole. The dihedral angles of the 3′-terminal segment, C74-C75-A76-D-Tyr, were modified to avoid clashes and to form favorable electrostatic and hydrophobic interactions. A tRNA orientation that permits potential interactions between phosphate groups and the conserved positively charged residues at positions 48*, 53*, 87, and 90 were selected (Fig. 5). Modeling was followed by energy minimization, moving only the tRNA 71–76-D-Tyr segment and imposing harmonic restraint on the distance between the Thr-80 O$^{\gamma}$ atom and the D-Tyr carbonyl carbon atom (modeled somewhat arbitrarily at 2.5 Å) to prevent repulsion because of the short contact expected to precede nucleophilic attack.

The key interactions in the active site are shown in Fig. 4*B*. The base-stacking interactions of the C74, C75, and A76 seen in the crystal structure of free tRNA are eliminated. Instead, a cluster of edge-to-face interactions is formed between the bases and the active site phenylalanine residues. The aromatic ring of the D-Tyr is also part of this cluster, stacking parallel to A76 and perpendicular to the benzene ring of Phe-79.

An ion pair interaction is formed between the invariant Arg7* and the A76 phosphodiester group. The O_2' hydroxyl of ribose 76 forms a hydrogen bond with the carbonyl oxygen of Pro-137*. Most strikingly, the amino nitrogen of D-Tyr is buried in an environment that is largely hydrophobic (Phe-93, Phe-140*,Val-138*, and Met-62*) with the exception of its interactions with the O_2 of the C75 base and with the Thr-80 Oγ atom. The position and orientation of D-Tyr amino group suggest that it binds in a deprotonated state by either dissipating a proton to solvent or donating it to the O_2 atom of C75. Therefore, D-Tyr amino group may serve as a general base, accepting a proton from the catalytic Thr-80 O$^{\gamma}$ atom.

The model of the complex reveals that the basis for discrimination in favor of D-amino acids is space exclusion, *i.e.* L-amino acids would clash badly with protein groups. On the other hand, any D-amino acid may be accommodated because the side chain projects toward solvent. The model explains another experimental observation, that is the enzyme is inactive

toward *N*-acetyl blocked D-aminoacylated tRNAs (2) because the amino group is buried in a crowded environment and additional atoms would not fit in the space.

The model indicates that catalysis is substrate-assisted (Fig. 6). The hydroxyl group of Thr-80 mounts a nucleophilic attack on the D-Tyr carbonyl carbon atom. The amino nitrogen atom of D-Tyr is deprotonated and is located in an appropriate position to accept a proton from Thr-80, thus serving as a general base. A negatively charged tetrahedral transition state is formed at the D-Tyr carbonyl carbon stabilized by the oxyanion hole. The D-Tyr-tRNA ester bond breaks, yielding an acyl enzyme. The tRNA molecule diffuses out of the active site, whereas the D-Tyr remains bound to the enzyme. A water molecule next attacks the acyl enzyme, replacing the departing tRNA ribose 76 O3′ atom, and the amino nitrogen atom of D-Tyr serves again as the base that accepts a proton from the activated water molecule. The ester bond between the enzyme and D-Tyr is cleaved, and free enzyme is generated for the next catalytic cycle. We note that substrate-assisted catalysis has been reported previously (19), and deprotonated amino groups have been observed in proteins when shielded from solvent (20).

The role of the invariant Ser-77 remains unclear. In both the *H. influenzae* and *E. coli* enzymes, Ser-77 is hydrogen-bonded to a water molecule (Wat265 and Wat1115 in the Protein Data Bank entries 1j7g and 1jke, respectively), which in turn is hydrogen-bonded to a second water molecule (Wat223 and Wat1384 in 1j7g and 1jke, respectively). Wat265 is also hydrogen-bonded to the main chain nitrogen of Ala-125, a residue on a type II reverse turn located on the edge of the active site depression. According to our model, neither of the water molecules needs to be displaced when the substrate binds and Wat223 is located ~5.5 Å from the modeled D-Tyr carbonyl carbon atom. It is tempting to speculate that Wat223 may serve as the hydrolytic water molecule and that Ser-77 hydroxyl group together with the main chain amide of Ala-125 and Wat265 help maintain the polar environment despite being somewhat shielded from the bulk solvent by the side chains of Phe-79 and Phe-124.

CONCLUSIONS

Detailed structural analyses and modeling provide the basis for the proposed catalytic mechanism of an important enzyme that helps maintain the fidelity of protein synthesis, D-Tyr-tRNA^{Tyr} deacylase. The modeled enzyme-tRNA complex is consistent with all of the available enzyme specificity data. The proposed catalytic pathway follows the general base mechanism seen in other hydrolytic enzymes. In the deacylase, Thr-80 hydroxyl serves as the nucleophilic group, there is an oxyanion hole to stabilize the negatively charged tetrahedral transition state, and the reaction is substrate-assisted by the amino group of D-Tyr, providing a “proton park” for the Thr-80 hydroxyl group. The enzyme-tRNA complex model and the proposed catalytic mechanism could not be developed without an accurate atomic structure of the enzyme. Moreover, the model suggests future experiments that should be carried out to elucidate the mechanism experimentally. Finally, the crystal structure of the enzyme-tRNA complex will reveal the exact interactions in the active site and validate or refute the proposed mechanism.

Acknowledgments

We thank John Moult and Eugene Melamud for the use and help with their bioinformatics web site (s2f.carb.nist.gov). We thank the staff of Industrial Macromolecular Crystallographic Association-Collaborative Access Team (IMCA-CAT) at the Advanced Photon Source for help during data collection. The IMCA-CAT facility is supported by the companies of the Industrial Macromolecular Crystallographic Association through a contract with Illinois Institute of Technology. The use of the Advanced Photon Source was supported by the U. S. Department of Energy, Basic Energy Sciences, Office of Science under contract W-31-109-Eng-38. The Keck foundation provided generous support for the purchase of x-ray equipment at Center for Advanced Research in Biotechnology.

REFERENCES

1. Calendar R, Berg P. J. Mol. Biol. 1967; 26:39–54. [PubMed: 4292198]
2. Soutourina J, Plateau P, Delort F, Peirotes A, Blanquet S. J. Biol. Chem. 1999; 274:19109–19114. [PubMed: 10383414]
3. Soutourina J, Plateau P, Blanquet S. J. Biol. Chem. 2000; 275:32535–32542. [PubMed: 10918062]
4. Soutourina J, Blanquet S, Plateau P. J. Biol. Chem. 2000; 275:11626–11630. [PubMed: 10766779]
5. Ferri-Fioni ML, Schmitt E, Soutourina J, Plateau P, Mechulam Y, Blanquet S. J. Biol. Chem. 2001; 276:47285–47290. [PubMed: 11568181]
6. Fleischmann RD, Adams MD, White O, Clayton RA, Kirkness EF, Kerlavage AR, Bult CJ, Tomb JF, Dougherty BA, Merrick JM, et al. Science. 1995; 269:496–512. [PubMed: 7542800]
7. Otwinowski Z, Minor W. Methods Enzymol. 1997; 276:307–326.
8. CCP4. Acta Crystallogr. Sec. D. 1994; 50:760–763.
9. Otwinowski, Z. Isomorphous Replacement and Anomalous Scattering. Wolf, W.; Evans, PR.; Leslie, AGW., editors. Daresbury Laboratory; Warrington, United Kingdom: 1991. p. 80-86.
10. Cowtan K. Joint CCP4 and ESF-EACBM Newsletter on Protein Crystallography. 1994; 31:34–38.
11. Perrakis A, Morris R, Lamzin VS. Nat. Struct. Biol. 1999; 6:458–463. [PubMed: 10331874]
12. Jones TA, Zou JY, Cowan SW, Kjeldgaard M. Acta Crystallogr. Sec. A. 1991; 47:110–119.
13. Brünger AT, Adams PD, Clore GM, DeLano WL, Gros P, Grosse-Kunstleve RW, Jiang JS, Kuszewski J, Nilges M, Pannu NS, Read RJ, Rice LM, Simonson T, Warren GL. Acta Crystallogr. Sec. D. 1998; 54:905–921.
14. Roussel, A.; Cambillau, C. TURBO-FRODO, version 4.3. Silicon Graphics; Mountain View, CA: 1989.
15. Shi H, Moore PB. RNA. 2000; 6:1091–1105. [PubMed: 10943889]
16. Holm L, Sander C. J. Mol. Biol. 1993; 233:123–138. [PubMed: 8377180]
17. Kraut J. Annu. Rev. Biochem. 1977; 46:331–358. [PubMed: 332063]
18. Herzberg O, Moult J. Science. 1987; 236:694–701. [PubMed: 3107125]
19. Dall'Acqua W, Carter P. Protein Sci. 2000; 9:1–9. [PubMed: 10739241]
20. Stites WE, Gittis AG, Lattman EE, Shortle D. J. Mol. Biol. 1991; 221:7–14. [PubMed: 1920420]
21. Kraullis PJ. J. Appl. Crystallogr. 1991; 24:946–950.
22. Bacon DJ, Anderson WF. J. Mol. Graph. 1988; 6:219–220.
23. Merrit EA, Bacon DJ. Methods Enzymol. 1997; 277:505–524. [PubMed: 18488322]
24. Altschul SF, Madden TL, Schaffer AA, Zhang J, Zhang Z, Miller W, Lipman DJ. Nucleic Acids Res. 1997; 25:3389–3402. [PubMed: 9254694]
25. Thompson JD, Higgins DG, Gibson TJ. Nucleic Acids Res. 1994; 22:4673–4680. [PubMed: 7984417]
26. Sanner MF, Olson AJ, Spehner JC. Biopolymers. 1996; 38:305–320. [PubMed: 8906967]

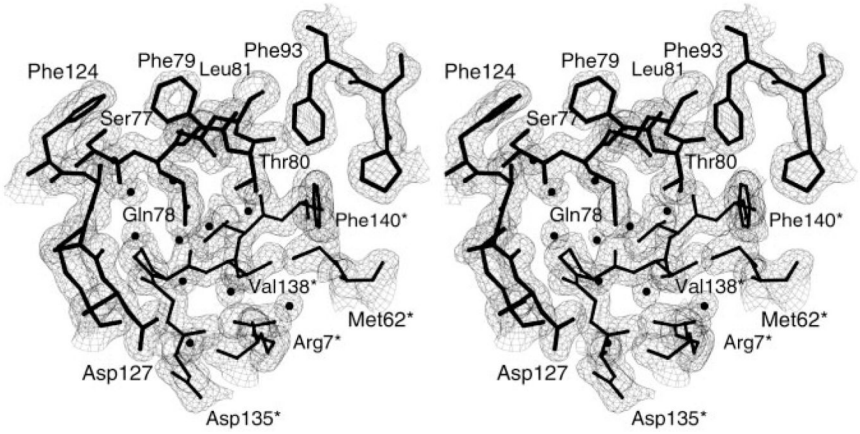

FIG. 1. Stereoscopic representation of the final electron density maps at a 1.64-Å resolution together with the model

The active site region is shown. The coefficients ($2F_o - F_c$) and calculated phases are used. The map is contoured at a 1σ level.

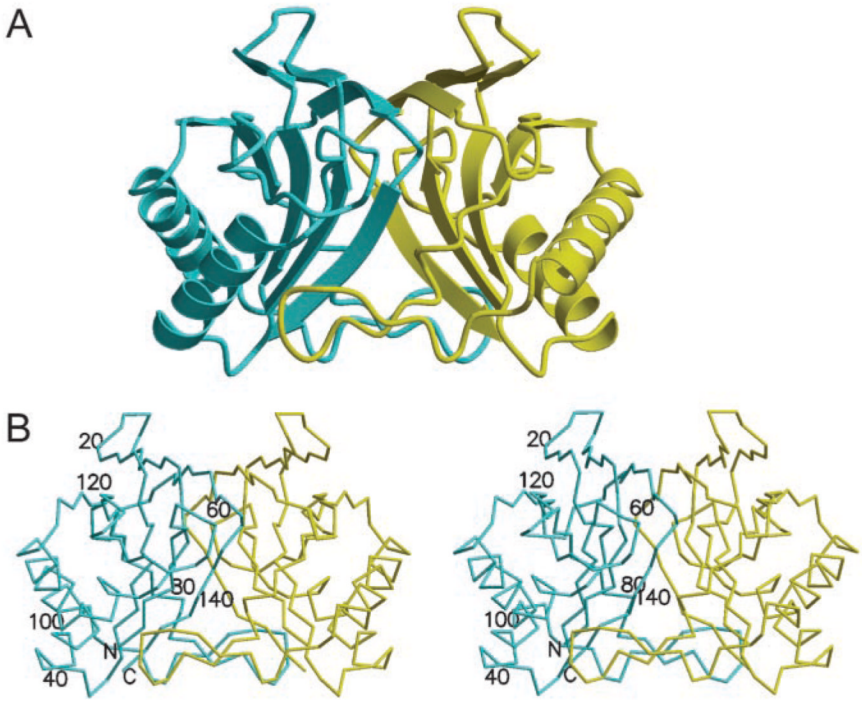

FIG. 2. Crystal structure of HI0670

A, ribbon diagram of a dimer with each monomer shown in a different color. *B*, stereoscopic representation of the Cα trace. Every 20th residue is labeled for one monomer. The figure was generated with the computer programs MOL-SCRIPT (21) and RASTER3D (22, 23).

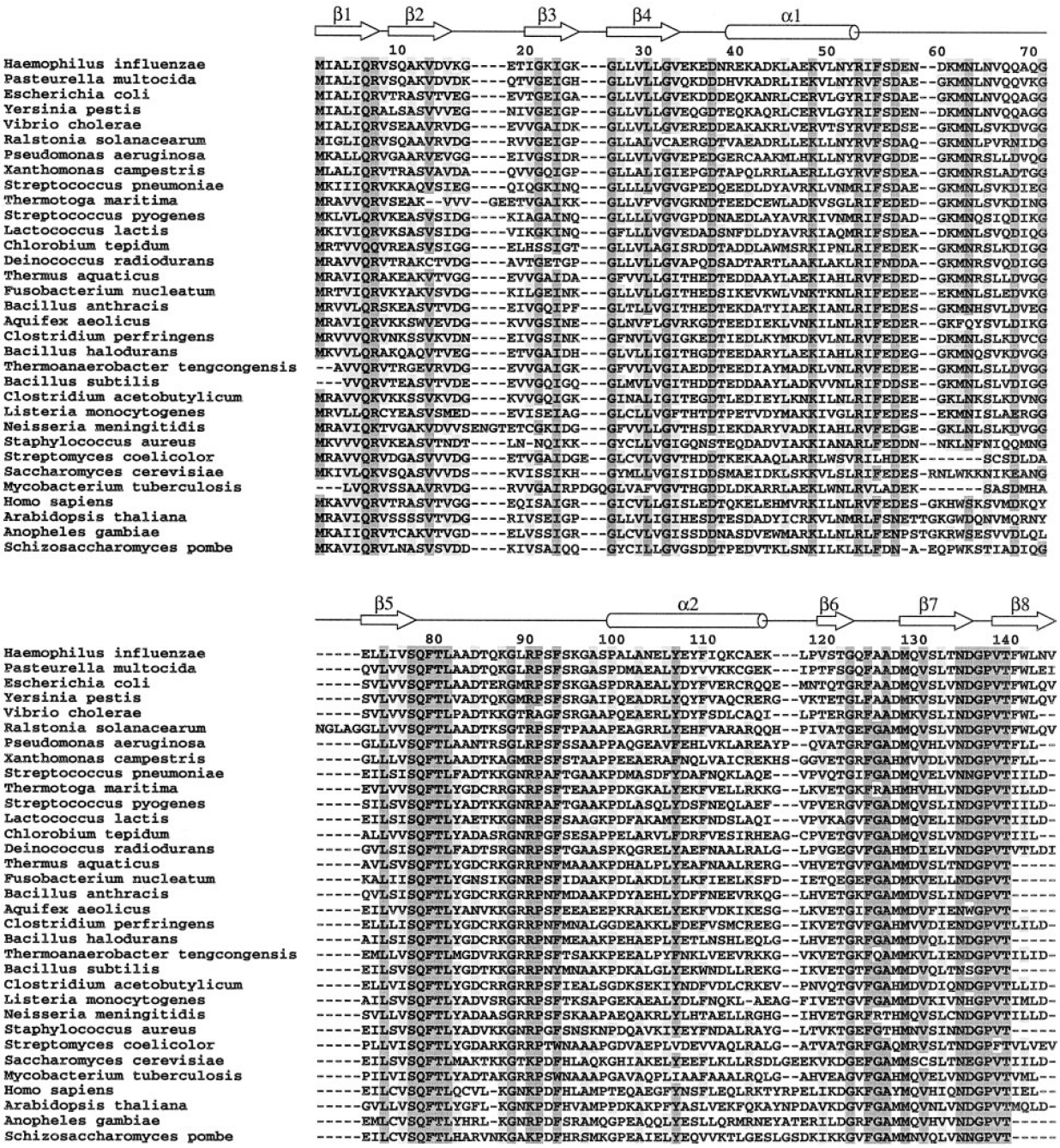

FIG. 3. Multiple sequence alignment of D-Tyr-tRNA^{Tyr} deacylase

At the time of writing, the first iteration of PSI-BLAST (24) using the NCBI non-redundant data base generates 57 homologous sequences. For brevity, only 33 sequences are shown. The alignment was constructed using ClustalW (25). The secondary structural elements of HI0670 are shown as *arrows* (*β*-strands) and cylinders (*α*-helices). Invariant residues are *shaded dark gray*, and conservatively replaced residues are *shaded light gray*. The proposed catalytic residue is Thr-80.

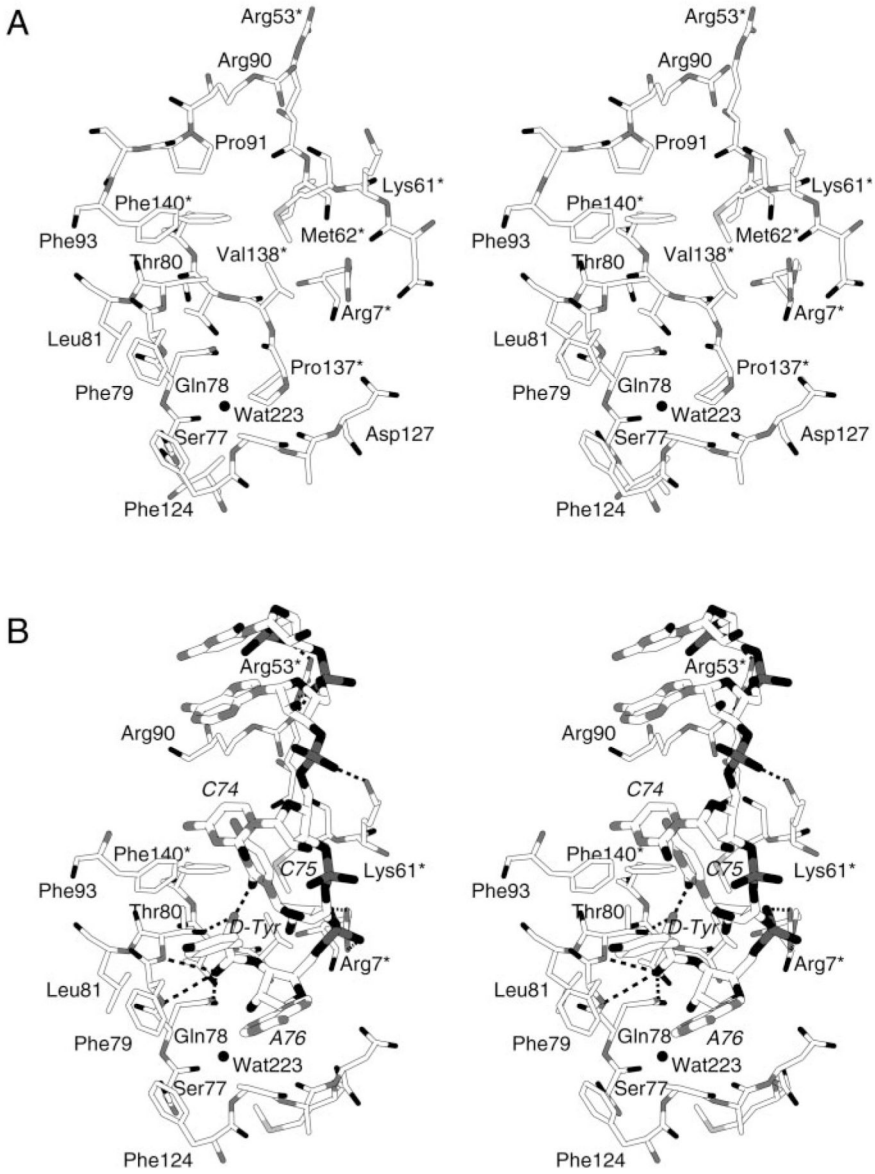

FIG. 4. Proposed active site of HI0670

A, spectroscopic representation of the residues forming the active site depression. Coloring scheme is as follows: oxygen atoms are shown in *black*; nitrogen atoms are shown in *gray*; and carbon atoms are shown in *white. B*, spectroscopic representation of a modeled D-Tyr-tRNA segment docked in the active site. The Thr-80 O^{γ} atom is oriented appropriately for nucleophilic attack on the carbonyl carbon of D-Tyr, and the carbonyl oxygen of D-Tyr is located in an oxyanion hole formed by the main chain nitrogen atoms of Phe-79 and Thr-80 and the side chain amide of Gln-78. These interactions, the two interactions of the amino group of D-Tyr (with Thr-80 O^{γ} atom and the O_2 of C75), and interactions between phosphate groups and positively charged protein residues are shown in *broken lines*. Coloring is as in noted in *A*, and in addition, phosphodiester phosphorus atoms are shown in *gray*. Wat223 is the water molecule closest to the carbonyl carbon of D-Tyr, which may perform the hydrolytic function. L-Tyr cannot be docked in this manner because its side

chain would replace the Cα proton and clash with several residues, in particular with the main chain of Thr-80.

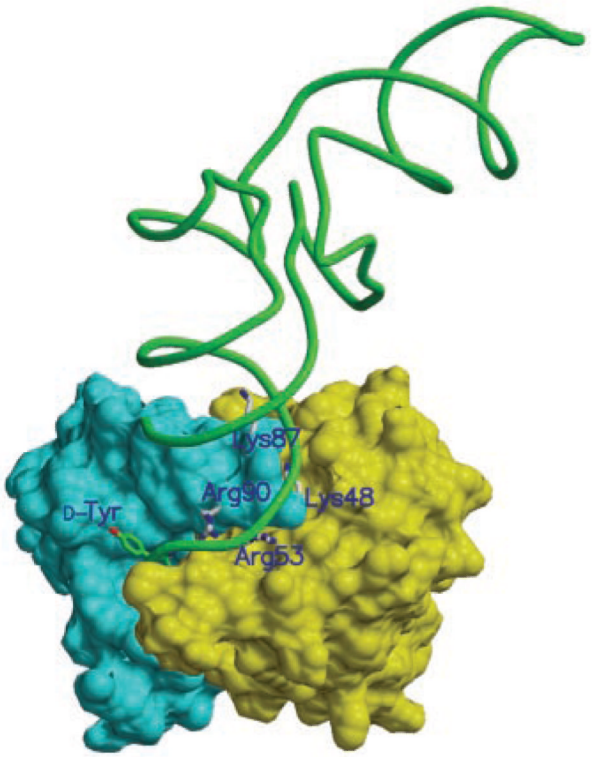

FIG. 5. A model of the complex between HI0670 and D-Tyr-tRNA

The molecular surfaces of the two monomers are shown in *blue* and *yellow colors*, and the tRNA molecule is shown as a *green coil*. The D-Tyr and four positively charged residues that interact with tRNA phosphate groups outside of the active site are shown as *stick models*. The molecular surface of the protein dimer was calculated with the computer program MCMS (26). The figure was generated with the computer program RASTER3D (22, 23). Note that the overall structure of the tRNA is that of $tRNA^{Phe}$, which is expected to be somewhat different from the structure of $tRNA^{Tyr}$. Thus, this is a rough model intended to demonstrate the feasibility of the proposed complex and to develop the proposed catalytic mechanism.

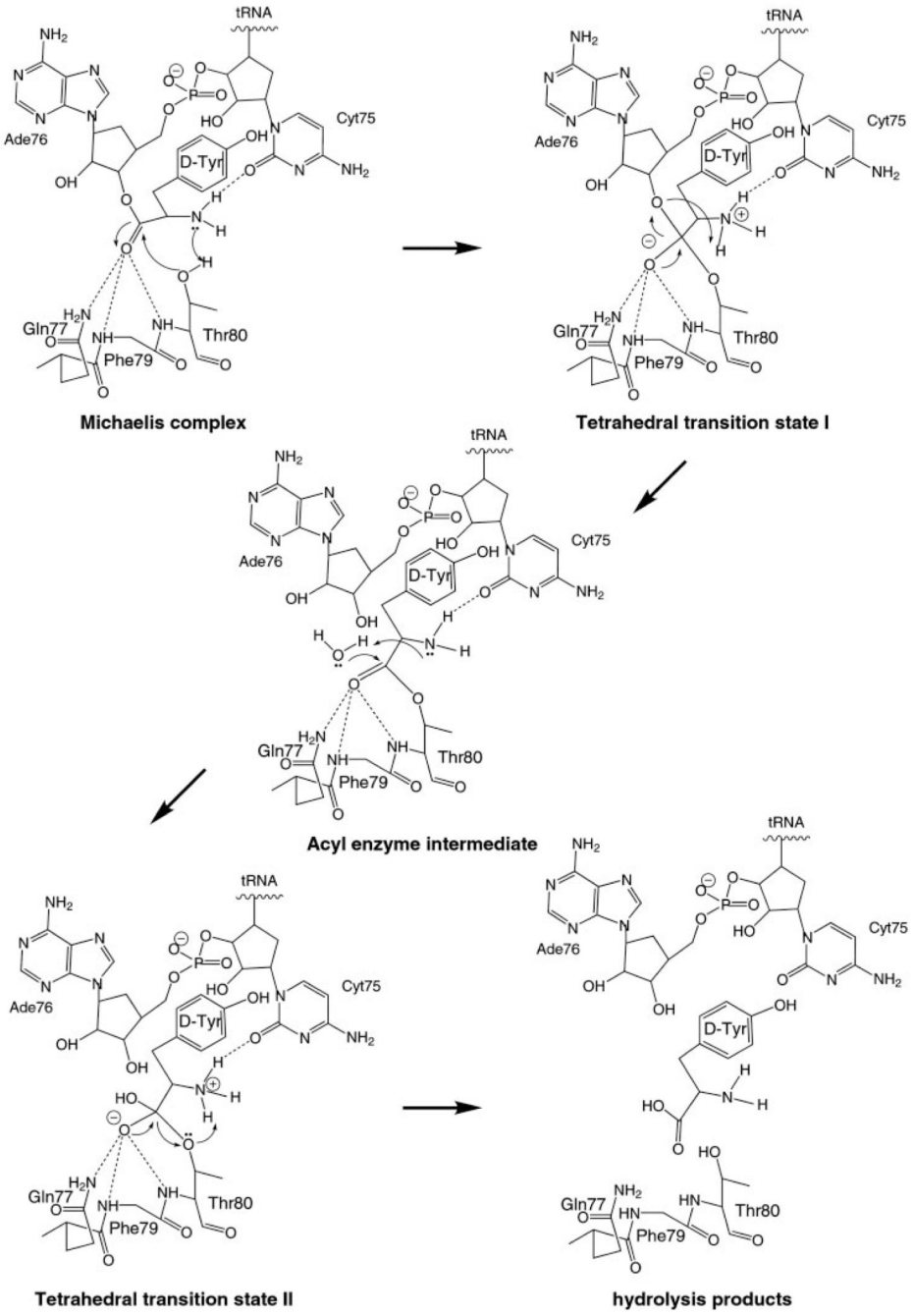

FIG. 6. A scheme of the proposed catalytic mechanism of D-Tyr-tRNA^{Tyr} deacylase deduced by docking a model of D-Tyr-tRNA in the proposed enzyme active site

Note that because the scheme is two-dimensional, the orientations and interactions of the D-Tyr side chain and of A76 are not depicted properly.

Table I

Data collection and phasing statistics

Space group		$P4_12_12$
Cell dimension (Å)		$a = b = 55.5$, $c = 128.8$
Number of molecules in the asymmetric unit		1
Crystals	Native	$(Ethyl\ Hg)_3PO_4$
Concentration (mM)		4
Length of soak (h)		48
Wavelength (Å)[a]	1.00	1.5418
Resolution (Å)	1.64	2.0
No. observed reflections	352,028	138,130
No. unique reflections	25,510	14,442
Completeness (%)[c]	99.8 (100.0)	99.7 (99.8)
R_{merge}[c]	0.037 (0.135)	0.100 (0.426)
$<I/\sigma>$	12.8	12.0
Phasing statistics		
Anomalous R[d]		0.79
Figure of merit		0.21

[a] Data at 1.54-Å wavelength were collected on the home X-ray facility, and data at 1.0 Å wavelength collected at IMCA-CAT beamline.

[b] The values in parentheses are for the highest resolution shell, *i.e.*, 1.71–1.64 Å for the native crystal and 2.09–2.0 Å for the $(ethyl\ Hg)_3PO_4$ crystal.

[c] $R_{merge} = \Sigma_{hkl}[(\Sigma_j|I_j - \langle I\rangle|)/\Sigma_j I_j]$.

[d] Anomalous $R = \Sigma_{hkl} | {}''F^{\pm}_{obs} - {}''F^{\pm}_{calc} | / \Sigma_{hkl} F^{\pm}_{obs}$, where ${}''F^{\pm}$ is the structure factor difference between Friedel pairs.

Table II

Refinement statistics

Resolution (Å)	20.0–1.64
Unique reflections $Fe\,2\sigma(F)$	23,308
Completeness (%)[a]	92.4 (74.5)
Number of protein atoms	1,115
Number of H_2O	207
R_{cryst} [b]	0.194 (0.237)
R_{free} [c]	0.220 (0.277)
r.m.s. deviation from ideal geometry	
Bond length (Å)	0.013
Bond angle (°)	1.8
Average B factor (Å^2)	
Protein	24
H_2O	42
Ramachandran plot (%)	
Most favored	89.1
Allowed	10.9
Generously allowed	0.0
Disallowed	0.0

[a] The values in parentheses are for the highest resolution shell.

[b] $R_{cryst} = \Sigma_{hkl} \| F_o| - |F_c| / \Sigma_{hkl} |F_o|$, where F_o and F_c are the observed and calculated structure factors, respectively.

[c] R_{free} is computed from 1,352 reflections that were randomly selected and omitted from the refinement.